AJNR

MR imaging of orbital and ocular disease.

D F Sobel, W Kelly, B O Kjos, D Char, M Brant-Zawadzki and D Norman

MR Imaging of Orbital and Ocular Disease

David F. Sobel[1]
William Kelly[1]
Bent O. Kjos[1]
Devron Char[2]
Michael Brant-Zawadzki[1]
David Norman[1]

Magnetic resonance (MR) images of 27 patients with ocular and orbital pathology were reviewed retrospectively and correlated with computed tomography (CT), funduscopic examination, and tissue histology. Disease processes were classified by location into ocular, extraconal, intraconal, optic nerve, and orbital apex. The diagnostic efficacy of MR differed at each location. MR was very sensitive in detecting ocular, extraconal, and intraconal lesions larger than 5 mm but was insensitive in imaging smaller lesions and in detecting pathology of the optic nerve. The limitations of MR were related to 7 mm slice thickness and 2.6 mm interslice gap. The diagnostic accuracy is expected to improve markedly with further developments in thin-section imaging and use of surface coils.

The potential of magnetic resonance (MR) imaging in evaluation of ophthalmologic disease has been discussed in preliminary reports from several centers including our own [1–4]. Images of the orbital structures demonstrated tissue contrast to be comparable or superior to high-resolution computed tomography (CT), whereas spatial resolution was inferior. Continuing clinical efforts and improved instrument design have allowed further evaluation regarding the diagnostic accuracy of MR; we herein report our experience.

Subjects and Methods

Twenty-seven patients were studied (table 1), with an age range of 4 months to 81 years. Four were included in a prior report describing our preliminary experience [1]. Fifteen were female and 12 male. Ocular pathology included choroidal melanoma (six patients), melanocytoma (one patient), retinoblastoma (one patient), and adenocarcinoma metastatic to the choroid (one patient). The four extraconal lesions comprised adenoid cystic carcinoma, adenocarcinoma, lymphocytic lymphoma, and dermoid, all in the lacrimal fossa. Intraconal lesions were orbital pseudotumor (three patients) and lymphangioma (two patients). Optic nerve pathology included bilateral optic nerve gliomas associated with neurofibromatosis (one patient), optic neuritis (three patients), and pseudotumor cerebri (three patients). Orbital apex disease was present in one patient with metastatic squamous carcinoma and another with Tolosa-Hunt syndrome.

MR images were obtained with a 0.5 T superconducting magnet operating at 0.35 T (Diasonics MT/S) with a resonant frequency of 15 MHz. Multislice spin-echo (SE) technique was used with variable repetition time (TR) settings of 500–2000 msec. Two images at 28 and 56 msec echo delay (TE) were acquired at each slice location. SE images are referred to as SE TR/TE and expressed in milliseconds. T1 and T2 data were calculated for those lesions studied with two different TR intervals and occupying sufficient pixel volume to eliminate partial-volume-averaging effect. T1 and T2 parameters were calculated from the equation, $I = (N[H]e^{-TE/T2})(1 - 2e^{-[TR-3TI]/T1} + 2e^{-[TR-TI]/T1} - e^{-TR/T1})$, where I = signal intensity, N(H) = resonating proton density, T1 and T2 are the exponential relaxation constants, TR is the pulse interval, TE is the echo delay, TI is the time of first 180° radiofrequency (RF) pulse, and 3TI is the time of the second 180° RF pulse. It should be noted that this is a more complete and accurate equation than that used for similar calculations in our early experience [5]. T1

SOBEL ET AL.

TABLE 1: **Ocular and Orbital Pathology Imaged by Magnetic Resonance**

Location: Pathologic/Clinical Diagnosis	No. of Patients	No. Biopsy-Proven
Ocular:		
Choroidal melanoma	6	3
Melanocytoma	1	0
Choroidal metastasis (adenocarcinoma of the lung)	1	0
Retinoblastoma	1	1
Extraconal:		
Lacrimal gland adenocarcinoma	1	1
Lacrimal gland adenoid cystic carcinoma .	1	1
Dermoid	1	1
Lymphocytic lymphoma	1	1
Intraconal:		
Orbital pseudotumor	3	3
Lymphangioma	2	2
Orbital apex:		
Tolosa-Hunt syndrome	1	1
Metastatic carcinoma (squamous cell) . . .	1	1
Optic nerve:		
Optic neuritis	3	0
Pseudotumor cerebri	3	0
Bilateral optic glioma	1	0
Total	27	

TABLE 2: **T1 and T2 Values in Patients with Ocular and Orbital Lesions**

Diagnosis	Calculated Value in msec (SD)	
	T1	T2
Melanoma	534	61
	548	67
	690	63
	572	65
	625	54
Lymphangioma	1134	123
Adenoid cystic carcinoma	849	79
Lymphoma	799	61
Normal ocular vitreous	2800 (426)	160 (92)
Normal orbital fat	290 (36)	57 (3)

and T2 values were measured in five of six melanomas and in three orbital tumors.

Results

The conspicuity of ocular and orbital structures was enhanced by the remarkable image contrast produced by inherent signal intensity differences between vitreous, fat, muscle, and neural tissue. Such intensity differences were based on the tissues' disparate T1/T2 relaxation and spin density values.

Ocular Lesions

Six patients had choroidal melanomas ranging in diameter from 3 mm to half the diameter of the globe. MR demonstrated all six lesions accurately (as did CT in the one patient in whom

it was performed). Melanomas tended to have relatively short T1 behavior, presumably due to the paramagnetic properties of melanin (table 2). For this reason, these lesions exhibited the greatest contrast with surrounding tissues on the SE 500/28 sequence, which allows T1 relaxation differences to contribute strongly to image contrast (fig.1). On the T2-weighted sequences, SE 1500 or 2000/56, five of six melanomas increased in relative intensity compared with brain or muscle but not compared with the ipsi- or contralateral vitreous, which also tended to increase in relative signal intensity. One melanoma actually decreased in relative intensity on SE 2000/56 images, reflecting faster T2 decay than the five other melanomas studied. Of interest, this lesion was clearly the most pigmented melanoma in this series.

Absolute T1 and T2 relaxation times were calculated for five of the six choroidal melanomas. The mean T1 value was 594 msec, and the mean T2 was 52 msec with standard deviations of 10% and 7%, respectively. The T1 values were significantly lower than those generally observed in other malignant neoplasms occurring in the brain. The T2 values likewise were quite short.

Foci of increased relative signal within the posterior globe were observed adjacent to three of the melanomas on T2-weighted sequences. These foci were distinguishable from the tumors by virtue of their lower intensity on the SE 500/28 sequence (due to their longer T1 relaxation). Pathologically, such foci represented subretinal fluid collections beneath detached retinas (figs. 1C and 1D).

A 2–3 mm melanocytoma of the optic nerve head seen funduscopically was not shown by MR imaging. We expected this lesion to be conspicuous based on its dense melanin pigmentation. The lack of visualization most likely reflected the 2.6 mm gap between consecutive sections obtained with our imager.

The retinoblastoma was well shown by both short and long TR SE sequences (fig. 2). Based on intensity characteristics relative to the vitreous and extraocular muscles, this lesion behaved in a manner similar to the melanomas. Unfortunately, T1 and T2 values could not be determined accurately for this lesion due to its small size. We would predict the T1 of the retinoblastoma to be in the range of other nonmelanotic, nonhemorrhagic malignancies. Of note, focal calcification in this lesion was detected easily by CT but was not visible with MR.

A 3 mm choroidal metastasis from adenocarcinoma of the lung was initially diagnosed funduscopically and appeared as a focus of increased signal relative to the vitreous on SE 2000/28 and 56 msec images.

Extraconal

The extraconal lesions all involved the lacrimal fossa and included an adenoid cystic carcinoma, adenocarcinoma, lymphoma, and dermoid. MR and CT were equal in imaging each of these masses. The presence of fat within the dermoid enabled a specific diagnosis to be made with both imaging techniques, due to the very high intensity (T1 = 300 msec) on MR and decreased x-ray attenuation on CT (fig. 3). The lacrimal carcinomas and lymphoma (fig. 4) could not be distin-
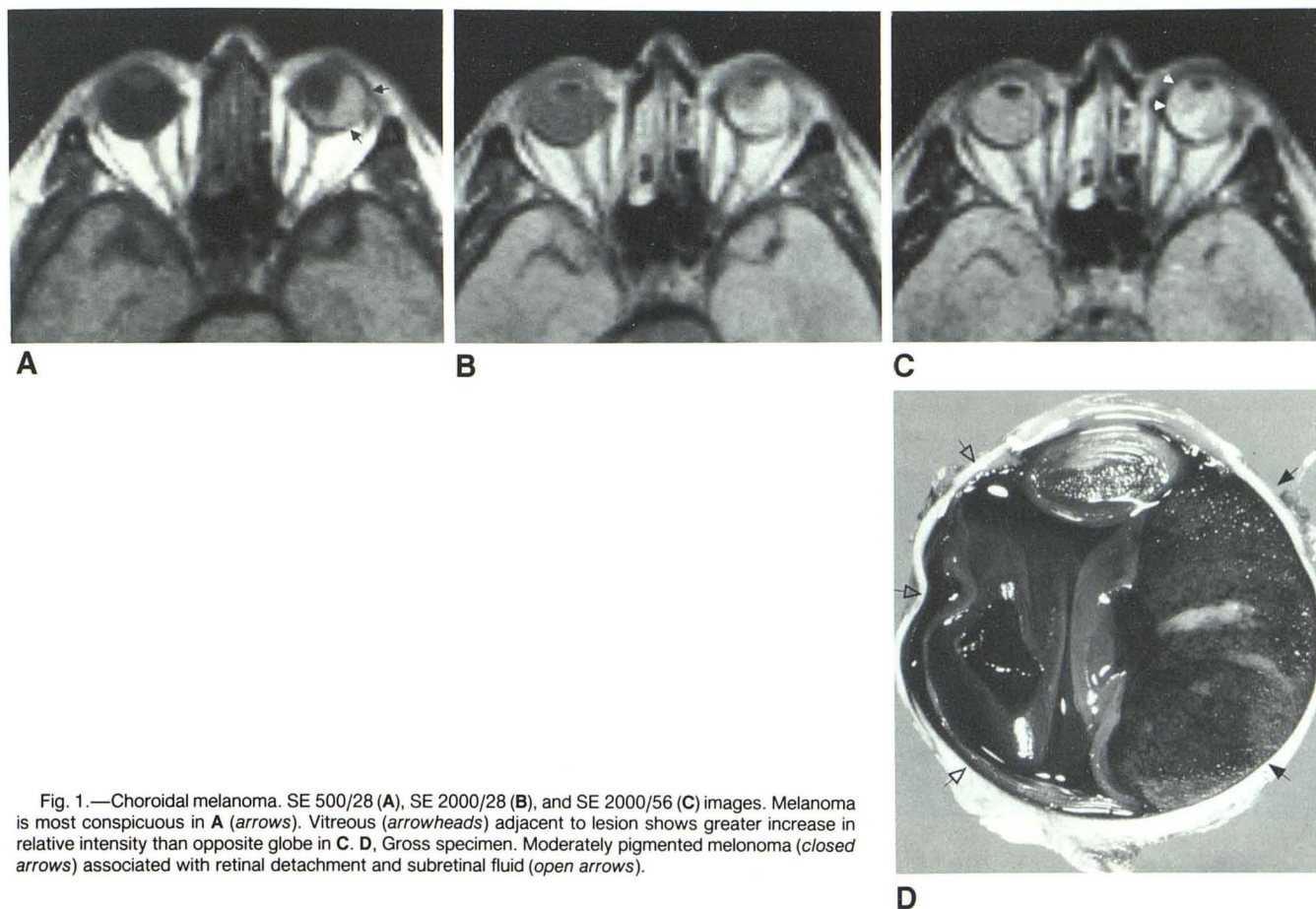
A　　　　　　　　　　　　　B　　　　　　　　　　　　　C

Fig. 1.—Choroidal melanoma. SE 500/28 (A), SE 2000/28 (B), and SE 2000/56 (C) images. Melanoma is most conspicuous in A (arrows). Vitreous (arrowheads) adjacent to lesion shows greater increase in relative intensity than opposite globe in C. D, Gross specimen. Moderately pigmented melonoma (closed arrows) associated with retinal detachment and subretinal fluid (open arrows).

D
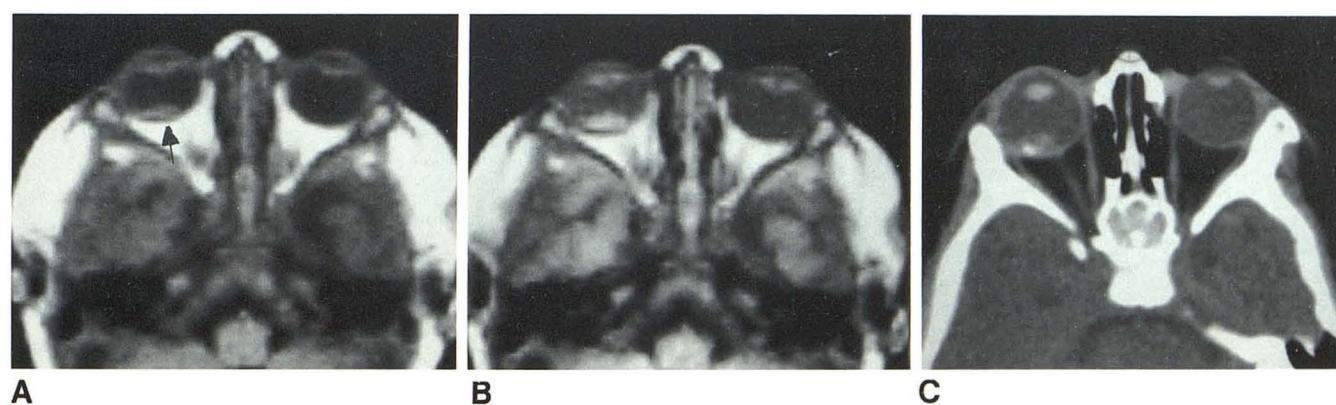

A　　　　　　　　　　　　　B　　　　　　　　　　　　　C

Fig. 2.—Retinoblastoma. SE 500/28 (A) and SE 1500/28 (B) images. Retinoblastoma is well imaged as focus of high signal intensity relative to vitreous (arrow). C, Unenhanced CT scan. Punctate calcification was not seen on MR images.

guished from each other based on intensity characteristics or relaxation parameters. Osseous destruction was helpful in suggesting the aggressive nature of the adenocarcinoma.

Intraconal

Three patients with orbital pseudotumor were studied. Findings in these patients have been reported [1]. Thickening of the rectus muscles and infiltration of the retorbulbar fat were well shown on MR and CT in all cases. Orbital fat normally yields a relatively strong signal due to its short T1 relaxation. In the presence of a relative edematous process such as an infiltrative pseudotumor, the T1 relaxation of fat is lengthened, resulting in decreased signal intensity. The T2 relaxation of involved fat was only slightly prolonged. Thus, the relative signal intensity of orbital pseudotumor exhibited minimal
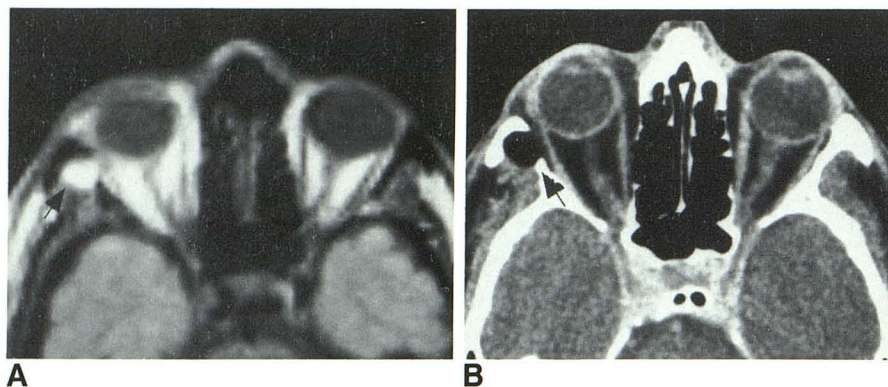
Fig. 3.—Dermoid of lacrimal fossa. SE 500/28 image (A) and contrast-enhanced CT scan (B). Dermoid (arrows) has same appearance as retrobulbar fat on both MR and CT. Erosion of lateral orbital wall is well shown by both.
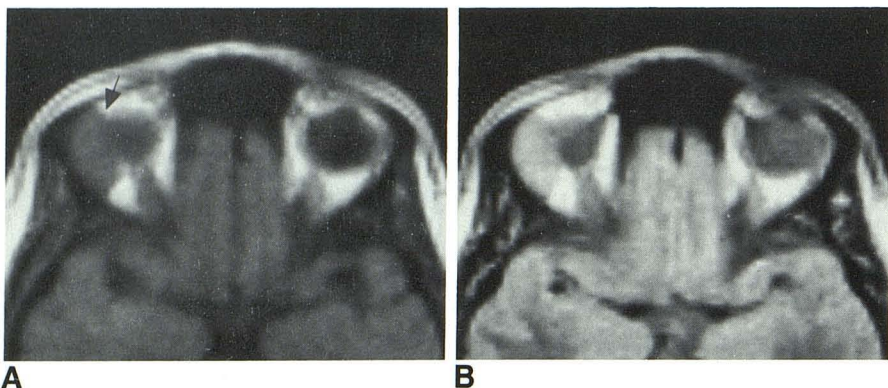

Fig. 4.—Lymphocytic lymphoma. SE 500/28 (A) and SE 1500/56 (B) images. Lesion seen best in A (arrow) due to its greater image contrast dependence on T1 relaxation time.
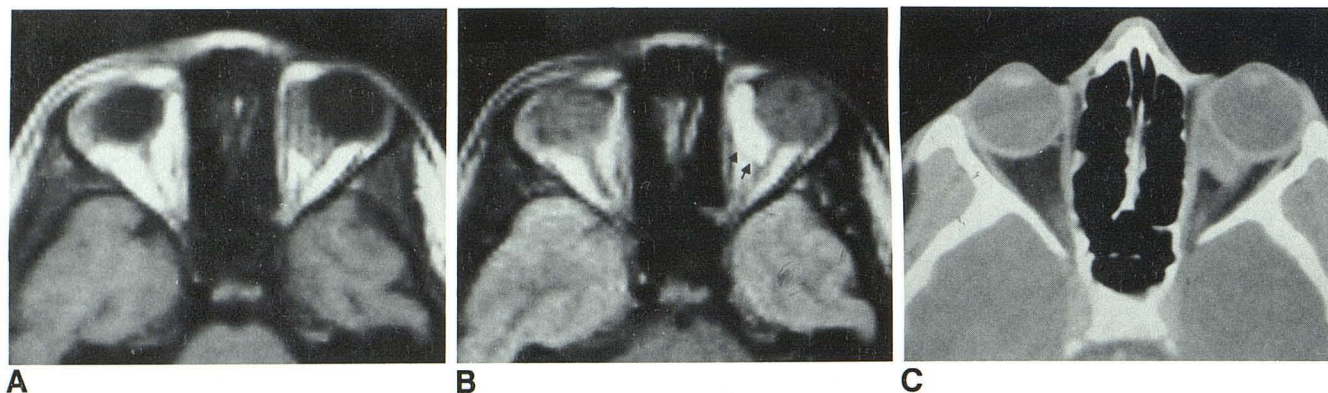

Fig. 5.—Lymphangioma. SE 500/28 (A) and SE 1500/56 (B) images and contrast-enhanced CT scan (C). Lymphangioma is relatively low in intensity on short TR, TE sequence (A) and is much brighter in relative intensity on long TR, TE image (B). Capsule (arrows) of lesion separates it from retrobular fat (B).

change between the 28 and 56 msec echoes.

The two lymphangiomas had similar or decreased intensity relative to fat on T1-weighted images. However, on the T2-weighted sequence they displayed brighter signal than the fat, due to the effect of their long T2 relaxation (fig. 5). A low-intensity capsule of these lesions demonstrated on the SE 2500/56 image was not observed on CT.

Orbital Apex

Lesions of the orbital apex were a granulomatous mass in a patient with Tolosa-Hunt syndrome and one carcinoma originating from the maxillary sinus and extending through the inferior orbital fissue to the orbital apex. The carcinoma appeared intermediate in signal intensity (in the range of

Fig. 6.—Bilateral optic nerve gliomas. SE 2000/28 image (A) and contrast-enhanced CT scan (B). Bilateral optic nerve enlargement is shown in B. MR images failed to demonstrate abnormalities.

A　　　　　　　　　　　　　B

muscle or neural tissue) on MR. The degree of extension and bone destruction were well shown on both MR and CT.

Granulation tissue applied to the greater wing of the sphenoid bone was found at surgery in the one pateint with Tolosa-Hunt syndrome. This finding was better shown preoperatively by CT but was also present on MR, where it appeared as a focus of decreased signal relative to brain. The low intensity on both T1- and T2-weighted sequences presumably reflected the relatively low resonating proton density of fibrous tissue.

Optic Nerve

MR was negative in bilateral optic nerve gliomas (one patient), optic neuritis (three patients), and pseudomotor cerebri (three patients). Failure of MR to detect the optic gliomas, which were shown on CT, is explained by an excessive slice thickness of 7 mm and spatial blurring from the high signal intensity of fat (fig. 6). Although MR and CT both failed to demonstrate optic nerve findings in optic neuritis, foci of abnormal high intensity in the periventricular white matter of the three patients studied were shown with MR, thus supporting the diagnosis of multiple sclerosis in these three patients.

Discussion

At the time of our study, the conspicuity of ocular and orbital lesions was limited mainly by our imager's ability to spatially resolve anatomic structures rather than its capacity to detect subtle alterations in tissue relaxation parameters and contrast. As with CT, tissue contrast of the orbital contents is excellent. Orbital fat, optic nerve, muscle, and vitreous have widely disparate T1 and T2 relaxation times and resonating proton densities, thus yielding markedly different signal intensity profiles resulting in high tissue contrast at commonly used operating frequencies and imaging sequences. The conspicuity of a pathologic lesion is also dependent on the ability to spatially resolve the abnormality. The false negatives in our study were due to lesions of small diameter situated within the interslice gap of 2.6 mm or occupying too few pixels to be detected with 7 mm section thickness. Improved spatial

resolution will occur with development of surface coils and thin-section technique. This will result in greater sensitivity in detecting small mass lesions and pathologic processes of the optic nerve. Alterations in T1 and T2 relaxation times may then play a paramount role. At present, the slice thickness of our imager is greater than the diameter of the optic nerve, extraocular muscles, and sclera. As a result signal-intensity measurements and relaxation time calculations are unreliable secondary to partial-volume averaging. Only larger masses or anatomic structures of sufficient volume may be accurately measured at this time.

Although MR detected eight of the nine ocular lesions, the 7 mm sections and 2.6 mm gap between sections used during this study limited the sensitivity to small lesions. Another significant shortcoming of MR was its failure to detect focal calcification seen on CT in the retinoblastoma, since calcification is sometimes the only radiographic clue to this diagnosis. Choroidal osteoma, phthisis bulbi, optic nerve head drusen, and traumatic displacement of cortical bone fragments are additional causes of calcification or ossification that may be missed when small in size. Large foci of calcification can often be detected by the paucity of signal on T1- and T2-weighted sequences due to the relatively low proton spin density.

The T1 properties of melanomas should lend some specificity in differentiating this tumor from other malignancies. Differentiating benign conditions such as melanocytoma may prove more difficult. The observation of relatively short T2 relaxation behavior in the most pigmented melanoma is based on the known shortening of T2 relaxation and the resulting effect on signal intensity with increasing concentration of paramagnetic substances [6, 7]. Melanin is a free radical that exhibits paramagnetic behavior due to an unpaired electron. This results in enhanced (shortened) T1 and T2 relaxation times. The degree of proton relaxation time shortening has been shown to be dependent on the concentration of the paramagnetic substance present. Hemorrhage, frequently present in melanomas, exhibits faster T1 relaxation (in the range of normal cerebral white matter, 400–600 msec) when in the nonacute stage than surrounding neoplastic tissue. Differentiation from neoplastic tissue with paramagnetic behavior is facilitated by the longer T2 and high proton spin

density of nonacute hemorrhage. Acute hemorrhage differs in having a relatively long T1 relaxation time.

MR accurately imaged all four extraconal processes, but as was the case with CT, exhibited little specificity except for the fat-containing dermoid. A surprising sensitivity to bone destruction was observed, even though paucity of resonating protons within cortical bone generates little signal. The black appearance of the orbital wall is normally highlighted by the stronger signal emitted from surrounding tissues. Thus, bone invasion or destruction is seen readily by the presence of emitted signal breaching the black-rimming cortical bone.

The intraconal processes in our series were accurately defined by MR imaging. The sensitivity of this technique in diagnosing orbital pseudotumor has been discussed [1]. The relatively long T2 relaxation time recorded in the two lymphangiomas served to differentiate these lesions from orbital pseudotumor. The long T2 is most likely attributable to fluid content. In one of these lesions pathologic examination revealed an admixture of lymphangioma and hemangioma. Slowly flowing or nearly stationary blood in the lateral component would tend to augment relative signal strength on the second echo of T2-weighted sequences.

MR was distinctly unrewarding in evaluating the optic nerve and its sheath. Again, the usage of excessive slice thickness hinders detection of subtle anatomic changes that should become more detectable with the forthcoming introduction of 1.8 mm section capability into our imager. In addition, spatial blurring resulting from the strong signal intensity generated by orbital fat may mask changes in signal intensity that might otherwise be detected, unless appropriate scaling is used. Daniels et al. [8] were able to image a glioma and meningioma of the intraorbital optic nerve with 5 mm MR sections, but the spatial resolution of these lesions with MR was inferior to that with CT.

Although coronal and sagittal images were not obtained in our study, they are readily available with MR multiplanar imaging and are now being incorporated in surface-coil studies of the orbit. Coronal planes of section are especially useful in avoiding partial-volume averaging when imaging the optic nerve.

In summary, MR was highly accurate in defining orbital and ocular lesions greater than 5 mm in size, but was insensitive in detecting smaller lesions. Similarly, MR was unrewarding in imaging optic nerve pathology using the current technique. MR was surprisingly able to demonstrate involvement of the osseous orbital wall, though we agree with others [3] that the definition is inferior to that of CT. Although a direct comparison with CT could not be made since CT was not performed in all patients, the diagnostic accuracy of CT in orbital imaging has already been established [9, 10]. At present, MR imaging offers no significant advantage over CT other than the absence of ionizing radiation. As surface coils and thin-section techniques become widely available, however, limitations of this imaging technique are expected to be overcome and a more realistic comparison between MR and CT in the evaluation of ophthalmologic disease will be undertaken.

REFERENCES

1. Sobel DF, Mills C, Char D, et al. NMR of the normal and pathologic eye and orbit. AJNR 1984;5:345–350
2. Moseley I, Brant-Zawadzki M, Mills C. Nuclear magnetic resonance imaging of the orbit. Br J Ophthalmol 1983;67:333–342
3. Han JS, Benson JE, Bonstelle CT, Alfidi RJ, Kaufman B, Levine M. Magnetic resonance imaging of the orbit: a preliminary experience. Radiology 1984;150:755–759
4. Gonzalez RG, Cheng HM, Barnett P, et al. Nuclear magnetic resonance imaging of the vitreous body. Science 1984;223:399–400
5. Ehman RL, Kjos BO, Brasch RC, Brant-Zawadzki M, Higgins CB. Spin echo imaging: method for correction of systematic errors in calculated T1 and spin density. Presented at the annual meeting of the Society of Magnetic Resonance in Medicine, New York City, August 1984
6. Brasch RC, Wesbey GE, Gooding CA, Koerper MA. Magnetic resonance imaging of transfusional hemosiderosis complicating thalassemia major. Radiology 1984;150:767–771
7. Damadian R, Zaner K, Hor D. Brain tumors by NMR. Physiol Chem Phys 1973;5:381–402
8. Daniels DL, Herfkins R, Gager WE. Magnetic resonance imaging of the optic nerves and chiasm. Radiology 1984;152:79–83
9. Char DM, Norman D. The use of computed tomography and ultrasonography in the evaluation of orbital masses. Surv Ophthalmol 1982;17:49–63
10. Forbes GS, Earnest F IV, Waller RR. Computed tomography of orbital tumors including late-generation scanning techniques. Radiology 1982;142:387–394